Hot Corrosion at Air-Ports in Kraft Recovery Boilers

Gordon R. Holcomb, Bernard S. Covino, Jr., and James H. Russell
Albany Research Center, U.S. Department of Energy

Abstract

Hot corrosion can occur on the cold-side of air-ports in Kraft recovery boilers. The primary corrosion mechanism involves the migration of sodium hydroxide and potassium hydroxide vapors through leaks in the furnace wall at the air-ports and their subsequent condensation. It has been reported that stainless steel is attacked much faster than carbon steel in composite tubes, and that carbon steel tubing, when used with a low-chromium refractory, does not exhibit this type of corrosion. For hot corrosion fluxing of metal oxides, either acidic or basic fluxing takes place, with a solubility minimum at the basicity of transition between the two reactions. For stainless steel, if the basicity of the fused salt is between the iron and chromium oxide solubility minima, then a synergistic effect can occur that leads to rapid corrosion. The products of one reaction are the reactants of the other, which eliminates the need for rate-controlling diffusion. This effect can explain why stainless steel is attacked more readily than carbon steel.

Introduction

The Kraft recovery boiler is a steam boiler used to recover process chemicals and to generate steam for paper-making and electricity generation. The fuel is spent liquor from the digester and contains dissolved organics.

Kraft boiler wall tubing typically consists *(1)* of co-extruded SA210 Gd A1 carbon steel with 1.5-1.8 mm (60-70 mils) of 304L on the outside diameter. Tube walls are constructed from either 7.62 cm (3") outer diameter (OD) tubes on 10.16 cm (4") centers or 6.35 cm (2.5") OD tubes on 7.62 cm (3") centers. The latter is shown in Fig.1.

The conditions in the Kraft recovery boiler are very corrosive and reported corrosion problems *(2)* include stress corrosion cracking, general corrosion, preferential corrosion of carbon steel welds, intergranular attack of stainless steel, and erosion corrosion. Corrosion of the boiler tubes at air-ports has also been a problem, especially at primary air-ports *(3-13)*. Although most instances of this type of corrosion have occurred at the primary air-ports, Barna and Rogan *(7)* have reported instances at the secondary air-ports. Bruno *(14)* has also reported similar corrosion above the secondary air-ports at the transition between the lower furnace composite tubes and the upper furnace carbon steel tubes (on the hot side of the tube wall).

Fig. 1: Section of Kraft recovery boiler tube wall of co-extruded SA201 Gd A1 carbon steel with 304L on the outside diameter. Kraft boiler tube wall courtesy of Oak Ridge National Laboratory.

Air-ports are where air is introduced into the boiler

through the water-cooled walls. Primary air-ports are located near the bottom of the boiler and supply about 40% of the oxygen needed for combustion *(3)*, so oxygen activity is quite low and the atmosphere is reducing. Higher in the boiler are secondary and tertiary air-ports and oxygen activity increases with further combustion.

Air-ports are gaps in the tube wall produced *(4)* by bending over a section of tube until it touches an adjacent tube. Designs include the cases where only one tube is bent and where adjacent tubes are bent in opposite directions. The opening is then framed by an iron casting to protect the tubes from rodding damage. Various stud and membrane designs are used to prevent flue gas from escaping. However, the dimensions of ports on a given boiler can vary by as much as 1 cm *(5)*, so obtaining a good fit is difficult and leaks are quite common.

Localized corrosion of the primary air-ports occurs on the outside (windbox side) of the furnace walls, not on the fireside. The corrosion typically occurs near the top and bottom of the air-port, where the tubes are bent to form the gap in the tube wall.

The most commonly cited corrosion mechanism *(3-12)* involves the migration of sodium hydroxide (NaOH) and potassium hydroxide (KOH) vapor through the furnace wall at the air-ports and their subsequent condensation. When the conditions (primarily temperature and condensate composition) are such that the condensation products are molten, then the molten salt attacks the metal heat exchanger tubes. Temperatures on the windbox side of the air-port are not constant. Falat *(13)* shows mean temperatures of 300 to 340°C, with temperature excursions in excess of 550°C. The melting temperatures of NaOH and KOH are 320°C and 410°C respectively, and the (Na,K)OH eutectic is 170°C *(3)*. Carbonation can lower the melting temperature of NaOH to as low as the eutectic temperature of 285°C *(15)*

There is not total agreement on the hydroxide condensation/corrosion mechanism. The main arguments against it are that NaOH is not always detected in the deposits (Na_2CO_3 is found instead) and that equilibrium calculations show that Na_2CO_3 should be formed instead of NaOH. However, hydroxides are found in some deposits *(3,6)* and Odelstam *et al (6)* have shown that kinetic considerations can greatly limit the conversion of NaOH to Na_2CO_3.

There are also differing explanations as to how the hydroxide rich deposits are formed. Simple condensation of vapors through leaks at the air-ports would be expected to result in deposits with higher sulfur contents than what is observed *(3)*. Bruno *(3)* offers three scenarios: 1) residual alkalinity of the black liquor results in volatilization of the sulfur, either on the walls or during in-flight travel of liquor droplets, 2) combustion and pyrolysis of organic carbon, combined with high water vapor pressure decreases the oxygen and sulfur activities in the deposit to produce conditions to form the hydroxide phase, or 3) capillary effects and low surface tension of hydroxide liquid phases result in a separation of a liquid sulfur-depleted and hydroxide-rich phase from the ordinary Na_2S-Na_2SO_4-Na_2CO_3 deposits.

It is reported that stainless steel is attacked much faster than carbon steel in composite tubes *(1-4, 6-13)* and that nickel overlays can also be attacked *(13)*. It has also been observed that carbon steel tubing, when used with a low-chromium refractory, does not exhibit this type of corrosion *(7)*.

Laboratory studies by Colwell *(8)* have shown that carbon steel initially corrodes faster than stainless steel, but soon stops corroding while the stainless steel continues to corrode with linear kinetics, Fig 2.

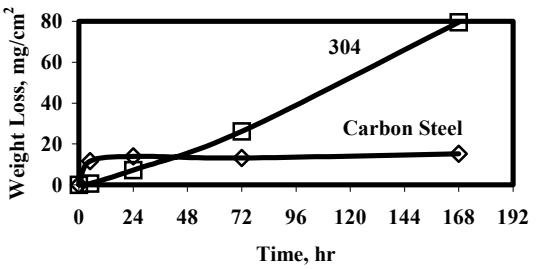

Fig. 2: Laboratory studies of 304 stainless steel and carbon steel exposed in a crucible of NaOH at 320°C under flowing dry air *(8)*.

After part of the stainless cladding on a co-extruded tube has corroded away, a galvanic mechanism has been proposed where the carbon steel is protected by the stainless steel, accelerating the attack on the stainless steel *(9-10)*. Tran *et al (9)* have measured electrochemical potentials in molten NaOH at 400°C and have found 304L to be anodic to carbon steel by about 170mV. However, Colwell *(8)* has reported that the measured galvanic currents were not sufficient to account for the difference in corrosion rates.

Hot corrosion theory will be used to give a possible explanation of why stainless steel corrodes faster than carbon steel. Initial experiments on the hot corrosion of Kraft boiler tube materials will also be presented.

Hot Corrosion Reactions

The corrosion attack by the (Na,K)OH-based molten salt is a form of hot corrosion, and hot corrosion has been extensively studied *(16-21)* in sodium sulfate ($NaSO_4$)-based molten salts in boilers and turbines. Hot corrosion is defined as the accelerated corrosion experienced by some metals and alloys when their surfaces are covered with a thin film of fused salt in an

oxidizing gaseous atmosphere at elevated temperatures *(16)*.

One of the main processes in the hot corrosion mechanisms is the dissolution, or "fluxing", of protective metal oxides and the subsequent exposure of the metal to the aggressive fused salt. Fluxing can proceed unabated if there is a negative solubility gradient within the fused salt away from the metal oxide (the Rapp-Goto criterion *(17)*). With a negative solubility gradient, metal oxides precipitate out within the fused salt, which acts as a sink for metal oxides and allows further dissolution of the protective oxide. With a positive solubility gradient, metal oxides build up in the fused salt and limit further dissolution of the protective oxide. Thus the solubility behavior of the metal oxide in the fused salt is important in describing hot corrosion behavior.

Oxyanion melts of sulfates and hydroxides exhibit an acid/base character analogous to aqueous solutions *(11-12,16)*. In the case of the hydroxide, MOH, where M equals Na or K, the dissociation is described by:

$$2MOH = M_2O + H_2O \quad (1)$$

where M_2O is the base component and H_2O is the acid component. Metal oxide fluxing can occur as either basic or acidic dissolution.

When the solubility of a metal oxide is plotted as a function of basicity (-log a_{Na2O}, or pNa_2O), and both basic and acidic dissolution takes place, then a solubility minimum occurs. This is illustrated in Fig. 3 with data at 500°C from Estes *et al*. *(11-12)* for Cr_2O_3 in NaOH. The data for Fe_2O_3 and NiO are also shown. In Fig. 3 the solubility axis is log concentration (ppm) of the moles of metal ions/moles of NaOH. For Cr_2O_3, the solubility minimum is at a pNa_2O of 8.2. No acidic dissolution was reported *(11-12)* for Fe_2O_3 in the basicity range tested. However, one would expect an acidic reaction at higher values of basicity. For NiO, no nickel was found in the melt below a pNa_2O of 8.3.

For the basic dissolution of Cr_2O_3 at a constant oxygen partial pressure, the reaction

$$Cr_2O_3 + 2O^{2-} + {}^3/_2O_2 = 2CrO_4^{2-} \quad (2)$$

is predicted to have a slope of -1 in Fig. 3 (log $[CrO_4^{2-}] \propto$ log $[O^{2-}] = -pNa_2O$). This is quite close to the experimental value of -0.99 *(11-12)*. For the acidic dissolution of Cr_2O_3 at a constant oxygen partial pressure, the reaction

$$Cr_2O_3 = 2Cr^{3+} + 3O^{2-} \quad (3)$$

is predicted to have a slope of ${}^3/_2$ in Fig. 3 (log $[Cr^{3+}] \propto -{}^3/_2$ log $[O^{2-}] \propto {}^3/_2$ pNa_2O), which is quite close to the experimental value of 1.48 *(11-12)*. Similar agreements between experiment and theory *(11-12)* support the following reactions for the basic dissolution of Fe_2O_3 (slope of -½) and the acidic dissolution of NiO (slope of 1):

$$Fe_2O_3 + O^{2-} = 2FeO_2^- \quad (4)$$

$$NiO = Ni^{2+} + O^{2-} \quad (5)$$

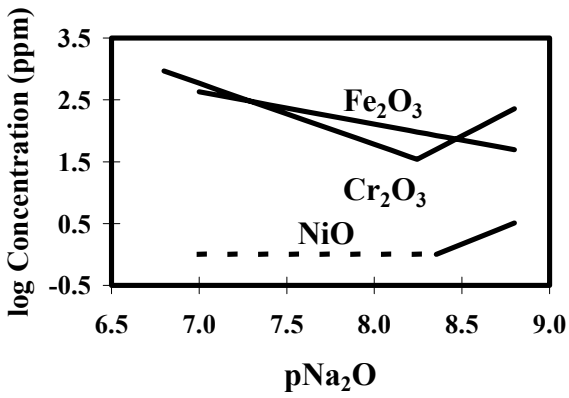

Fig. 3: Measured oxide solubilities in fused NaOH at 500°C as a function of basicity *(11-12)*. For NiO, no nickel was found in the melt below a pNa_2O of 8.3.

Synergistic Hot Corrosion

Studies *(16, 18)* of hot corrosion fluxing in Na_2SO_4 have shown that the reaction rate, when the Rapp-Goto criterion is satisfied *(17)*, is controlled by the diffusion of oxygen in the form of $S_2O_7^{2-}$. In basic solutions, it is diffusion to the protective oxide. In acidic solutions, it is diffusion away from the protective oxide.

When two metals together undergo hot corrosion, and the basicity is such that it is between the solubility minima of the two metal oxides, the corrosion kinetics can greatly increase *(18)*. This is because the products of one dissolution reaction are the reactants of the other, thus largely eliminating diffusion of oxygen as controlling the kinetics.

In the case of stainless steel in NaOH, when the basicity is above the Cr_2O_3 solubility minimum and below the Fe_2O_3 minimum (beyond the basicity range in Fig 3), a coupled reaction can be written that eliminates the need for the diffusion of O^{2-}. Equations (3) and (4) can be combined to form the coupled reaction:

$$Cr_2O_3 + 3Fe_2O_3 = 2Cr^{3+} + 6FeO_2^- \quad (6)$$

This coupled reaction, without the need for the kinetics to be limited by O^{2-} diffusion, could explain the

rapid localized attack of stainless steel at air-ports *(3-4, 6-13)*. It would also explain the observation that carbon steel is attacked much less when used with a lower chromium refractory *(7)*.

Falat *(13)* has reported attack of nickel overlays at air-ports, which is suggestive of an environmental basicity above 8.3. An environmental basicity above 8.3 would be above the solubility minimum of Cr_2O_3 and thus likely be in the basicity range described by Eq. 5. However, as the section "Controlling the Basicity" describes, reactions at the oxide-salt interface may control the basicity rather than the environmental basicity.

Experimental Procedures

The starting material used in initial hot corrosion experiments was a cross-section slice from the co-extruded tubes shown in Fig. 1. The cross-section was then cut to produce two small arcs of the tube wall. The arcs were then ground to 600 grit with parallel sides, Fig. 4. The widths of the parallel sides were measured for thickness-loss measurements.

The top faces of both samples were then coated with a thin layer of NaOH. The NaOH was placed on the samples by carefully applying two coats of NaOH saturated methanol. This resulted in a mean NaOH coating of 10 mg/cm^2, Fig. 5.

Fig. 4: Initial tube wall sample from a SA210 Gd A1 carbon steel and 304L co-extruded tube.

Fig. 5: A co-extruded sample with a NaOH coating.

The samples were exposed at 400°C for 72 hours in a flowing 20% O_2 – 80% N_2 atmosphere.

Results and Discussion

After exposure, the samples were allowed to cool in a N_2 atmosphere and removed from the furnace. For the most part, the NaOH salts remained on the surface as a white granular layer, Fig. 6. The NaOH salts were easily removed with washing to reveal the metal beneath, Fig. 7. The carbon steel had a dark reddish tinge and the 304L stainless was metallic gray.

Fig. 6: Duplicate co-extruded samples after hot corrosion at 400°C for 72 hours with NaOH remaining on the surface.

Fig. 7: Duplicate co-extruded samples after hot corrosion at 400°C for 72 hours and after NaOH removed. The carbon steel has a reddish tinge and the 304L is metallic gray.

The samples were then mounted with the outer pipe diameter facing downwards and ground down enough to reveal the carbon steel-304L interface. The carbon steel-304L interface is shown in Fig. 8. No morphological differences between the two metals were observed at the exposed surface. The exposed surface remained smooth and without any scale. This smoothness is in contrast to what one might expect from a galvanic effect, where the carbon steel in close proximity to the stainless steel would be protected at the expense of the stainless steel. The interface between the stainless and carbon steels shows good bonding between the two layers.

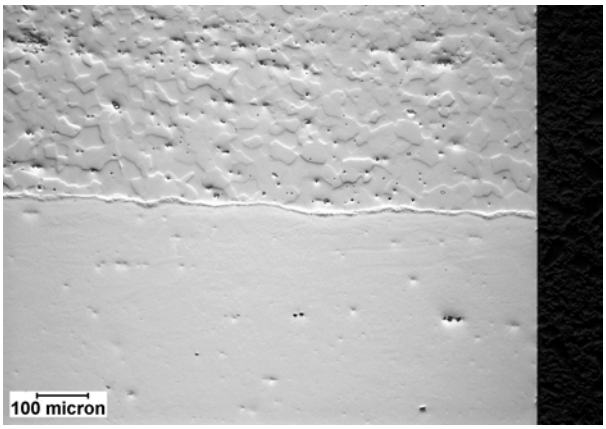

Fig. 8: A Cross-section showing the interface of the SA210 Gd A1 carbon steel (above) with the 304L coating (below) after exposure at 400°C for 72 hours with NaOH. The micrograph was taken using differential interference contrast. The sample was unetched.

Higher magnification images of the interface were taken using scanning electron microscopy and are shown in Fig. 9. The secondary electron image (top image) shows a layer of the carbon steel breaking away from the substrate. The stainless steel surface is generally much smoother than the carbon steel surface.

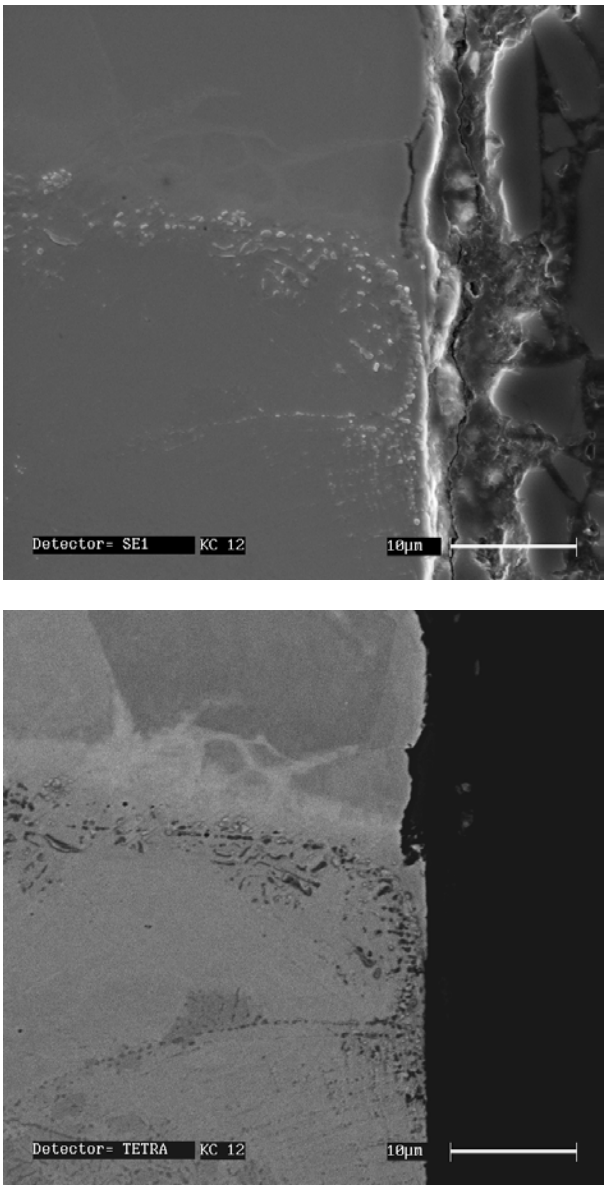

Fig. 9: Secondary electron (top image) and backscattered electron (bottom image) images of the cross-section showing the interface of the SA210 Gd A1 carbon steel (above) with the 304L coating (below) after exposure at 400°C for 72 hours with NaOH. The sample is unetched.

Thickness loss measurements were taken across the sample, with three measurements in the carbon steel section and four measurements in the stainless steel sections (two measurements across each of the two stainless steel sections obtained after mounting the sample as described above). The results are shown in Table 1

The differences between the carbon steel and 304L results were small, with, on average, a small increase in corrosion loss in the stainless steel as compared to the carbon steel. The results lie between the two curves in Fig. 2 at 72 hours of exposure.

Table 1. Thickness loss after exposure to NaOH at 400°C for 72 hours.

	Thickness Loss, µm	Calculated Mass Loss, mg/cm^2
Sample 1 Carbon Steel	26	20
Sample 2 Carbon Steel	20	15
Sample 1 304L	24	19
Sample 2 304L	30	24
Carbon Steel (mean)	23	18
304L (mean)	27	22

Controlling the Basicity

It would appear that if one could control the basicity of the environment, then hot corrosion could also be slowed. If the basicity is moved away from between the solubility minima for Cr_2O_3 and Fe_2O_3, then synergistic effects would be eliminated. However, it is not certain that controlling the ambient environment will change the local environment at the fused salt-protective oxide interface. For example, when pre-oxidized nickel was placed under a thin film of Na_2SO_4 in an acidic O_2-0.1% SO_2 gas environment at 900°C, simultaneous measurements of the sodium and oxygen activities showed that the local environment changed to basic conditions within 15 minutes *(16, 22)*. Thus, it was the local reactions at the fused salt-protective oxide interface that determined the basicity at the interface, not the overall environmental basicity. So, further investigation is needed to determine if environmental control can be effective in reducing hot corrosion at air-ports. In the case of corrosion in Na_2SO_4-based fused salts, low temperature "Type II" hot corrosion is very sensitive to the environmental basicity, while high temperature "Type I" hot corrosion is much less sensitive *(23)*.

Summary and Conclusions

Hot corrosion theory can explain the localized corrosion on the cold-side of air-ports in Kraft recovery boilers. Hot corrosion can occur by the dissolution, or fluxing, of the metal into the fused salt. Depending on the basicity, either acidic or basic fluxing takes place. There is a solubility minimum at the transition between the two reactions.

For the hot corrosion of alloys, if the basicity of the fused salt is such that it is between two metal oxide solubility minima, then a synergistic effect can occur that leads to rapid hot corrosion attack. This is due to the products of one reaction being the reactants of the other, which eliminates the need for rate-controlling diffusion of either one. This synergistic effect can explain why stainless steel is attacked more readily than carbon steel, and why carbon steel is not attacked in the presence of

low-chromium refractory.

Based on experience with Type I and II hot corrosion in Na_2SO_4, it is unclear if changing the atmospheric conditions would change the local basicity at the oxide-salt interface and the change the corrosion behavior.

The initial experimental results show a small increase in corrosion in 304L as compared to SA210 Gd A1 carbon steel in a cross-sectioned co-extruded pipe. However as Fig. 2 suggests, longer exposure times are needed to be more conclusive.

Acknowledgments

The authors wish to thank Jim Keiser from Oak Ridge National Laboratory for helpful discussions and for supplying the co-extruded Kraft boiler tubing used in this study.

References

1. J. R. Keiser, private communications, Oak Ridge National Laboratory, Oakridge, Tennessee (2001).
2. A. Wensley, "Corrosion Protection of *Kraft* Digesters," CORROSION/2001, paper 01423, NACE International, Houston, Texas (2001)
3. F. Bruno, *Pulp & Paper Industry Corrosion Problems*, Vol. 4, Proceedings of the Fourth International Symposium on Corrosion in the Pulp & Paper Industry, pp. 68-75, Swedish Corrosion Institute, Stockholm (1983)
4. D. A. Wensley, *Materials Performance*, 26(11), 53-55 (1987)
5. S. M. Cochrane, *International Chemical Recovery Conference*, Vol. 3, pp. 909-913, Tappi Press, Atlanta, Georgia (1998)
6. T. Odelstam, H. N. Tran, D. Barham, D. W. Reeve, M. Hupa, and R. Backman*, 1987 TAPPI Engineering Conference Proceedings*, Book 2, pp. 585-590, Tappi Press, Atlanta, Georgia (1987)
7. J. L. Barna and J. B. Rogan, *1986 TAPPI Engineering Conference Proceedings*, Book 2, pp. 377-385, Tappi Press, Atlanta, Georgia (1986)
8. J. A. Colwell, *Proceedings of the 7th International Symposium on Corrosion in the Pulp & Paper Industry*, pp. 231-241, Tappi Press, Atlanta, Georgia (1992)
9. H. Tran, N. A. Katiforis, T. A. Utigard, and D. Barham, *Tappi J.*, 78(9), 111-117 (1995)
10. M. A. Lunn, W. B. A. Sharp, J. D. Andrews, H. N. Tran, and D. Barham, *Proceedings of the 6th International Symposium in the Pulp and Paper Industry*, pp. 151-162, Tappi Press, Atlanta, Georgia (1989)
11. M. Estes, M. Marek, P. Singh, A. Rudie, and J. Colwell, *Proceedings of the Ninth International Symposium on Corrosion in the Pulp and Paper Industry*, pp. 231-235, Tappi Press, Atlanta, Georgia, (1998)
12. M. Estes, A. Rudie, P. Singh, M. Marek, and J. Colwell. *J. Pulp Paper Can.* 100(12), 106-109 (1999)
13. L. Falat, *Tappi J.*, 79(2), 175-185 (1996)
14. F. Bruno, *Proceedings of the 10th International Symposium on Corrosion in the Pulp and Paper Industry*, Ed. T. Hakkarainen, pp. 27-44, VTT Symposium Proceedings series no. 214 (2001)
15. R. P. Seward, *J. Amer. Chem. Soc*., 64, 1053-1054 (1942)
16. R. A. Rapp and Y. S. Zhang, *JOM* 46(12), 47-55 (1994)
17. R. A. Rapp and K. S. Goto, *Molten Salts I*, Eds. J. Braunstein and J. R. Selman, pp. 159-177, Electrochem. Soc., Pennington, New Jersey (1981)
18. Y.-S. Hwang and R. A. Rapp, *J. Electrochem. Soc.* 137, 1276-1280 (1990)
19. K. L Luthra, *Proceedings of the Symposium on High Temperature Materials Chemistry III*, Eds. Z. A. Munir and D. Cubbicciotti, pp. 212-216, Electrochemical Soc., Pennington, New Jersey (1986)
20. J. Stringer, *Ann. Rev. Mater. Sci.*, 7, 477-509 (1977)
21. F. S. Pettit and C. S. Gigins, *Superalloys II*, Eds. C. T. Sims, N. S. Stoloff, and W. C. Hagel, pp. 327-358, John Wiley & Sons, New York, New York (1987)
22. N. Otsuka and R. A. Rapp, *J. Electrochem. Soc.* 137, 46-52 (1990)
23. J. Stringer, *High Temperature Corrosion*, NACE-6, Ed. R. A. Rapp, pp. 389-397, National Association of Corrosion Engineers, Houston, Texas (1981)